

## Article

# Improve Ship Propeller Efficiency via Optimum Design of Propeller Boss Cap Fins

Chungen Yin <sup>1,\*</sup>, Christian Kjaer Roseninge <sup>1</sup>, Marcus Pless Sandland <sup>1</sup> , Anders Ehlers <sup>2</sup> and Keun Woo Shin <sup>2</sup><sup>1</sup> AAU Energy, Aalborg University, 9220 Aalborg East, Denmark<sup>2</sup> Propeller & Aftship R&D Department, MAN PrimeServ, 9900 Frederikshavn, Denmark

\* Correspondence: chy@energy.aau.dk; Tel.: +45-30622577

**Abstract:** This paper aims to cost-effectively improve the energy efficiency of large vessels in shipping by the optimum design of propeller boss cap fins (PBCFs). First, a model propeller of the modern four-blade propeller in a Ro-Ro ship, with no boss cap fin in its original design, is experimentally and numerically investigated. The computational fluid dynamics (CFD) model reproduced all the experiments very well. Then, the CFD model is used to conduct a comprehensive optimum design of PBCFs for the down-scaled propeller. Besides the commonly used rectangular PBCFs, nine airfoils are investigated, due to their favorable lift-to-drag ratio and great potential of being effective PBCFs. The best performing profile, among the 10 shapes, is chosen as the PBCF for further optimization. Finally, the optimum design of the PBCFs for the propeller/rudder system is achieved. It was found to yield remarkable efficiency gains for the modern propeller/rudder system under both design and off-design operation conditions, mainly due to the suppressed hub vortex and partly due to the extra thrust. The yield strength analysis confirmed that the optimum design is feasible in practice and can be used in industrial vessels. The generalized criteria for the optimum design of PBCFs also benefit other propeller/rudder systems for cost-effective energy saving.

**Keywords:** energy efficiency; shipping; CFD; cost-effective; propeller boss cap fins; optimization



**Citation:** Yin, C.; Roseninge, C.K.; Sandland, M.P.; Ehlers, A.; Shin, K.W. Improve Ship Propeller Efficiency via Optimum Design of Propeller Boss Cap Fins. *Energies* **2023**, *16*, 1247. <https://doi.org/10.3390/en16031247>

Academic Editor: Rob J.M. Bastiaans

Received: 2 January 2023

Revised: 18 January 2023

Accepted: 20 January 2023

Published: 23 January 2023



**Copyright:** © 2023 by the authors. Licensee MDPI, Basel, Switzerland. This article is an open access article distributed under the terms and conditions of the Creative Commons Attribution (CC BY) license (<https://creativecommons.org/licenses/by/4.0/>).

## 1. Introduction

As one of the most widespread transport modes, sea shipping accounts for nearly 3% of global greenhouse gas emissions, making it the 6th largest CO<sub>2</sub> producer in the world [1]. The growing concerns about emissions from shipping and fuel price push the shipping sector for new regulations. The International Maritime Organization (IMO) has set strict regulations to reduce gas emissions and improve energy efficiency. For example, a target was set in 2018 to reduce CO<sub>2</sub> emissions from the shipping sector by 70% by 2050, benchmarked to the 2008 levels [1]. The energy efficiency design index enacted by the IMO obligates newly manufactured shipping vessels to meet the minimum requirements on energy efficiency. There are various energy efficiency measures for ships, e.g., bow optimization [2], thrusters allocation optimization [3], main switchboard redimensioning [4], design of energy-saving ducts [5], smart speed adjustment [6], use of renewable energy and alternative fuels, operational measures optimization including various propeller/rudder designs, and so on [1]. These measures result in efficiency gains of different levels, which also demand investments of different levels.

Among the different energy saving measures, this paper focuses on aftship energy saving devices which demand little investment. These devices can be implemented at different regions, depending on their purposes. As shown in Figure 1, they can be implemented upstream of the propeller (Region I), to accommodate a more favorable wake to the propeller or to reduce drag. They can also be implemented in the propeller region (Region II), or in the rudder region (Region III), in both of which the devices are usually used either to lower the torque on the propeller shaft or to increase the thrust from the propeller blades.

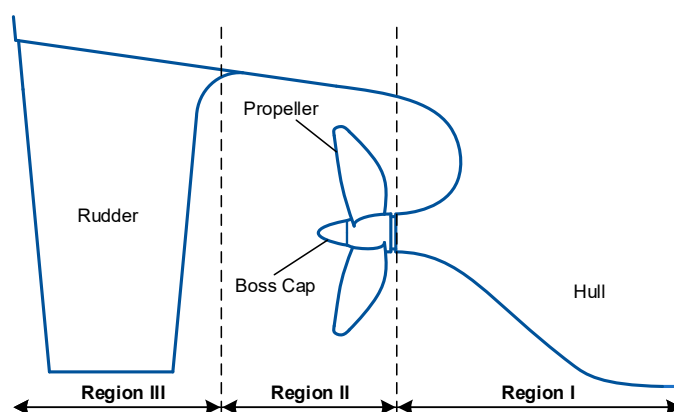


Figure 1. Classification of the regions for aftship energy saving devices.

Propeller boss cap fins (PBCFs) are a cost-effective aftship energy saving device and do not require vessel modification. PBCFs can weaken or eliminate the hub vortex created by propeller rotation, lower the torque on the propeller shaft, and increase the propeller efficiency. Here, the three key points for an efficient design of PBCFs, proposed in the first patent for PBCFs, are summarized. (1) The number of fins and propeller blades should stay the same, (2) the fin radius should be less than one-third of the propeller radius, and (3) the difference between the PBCFs installation angle and the propeller blade root pitch angle should be in the range of  $-20^{\circ} \sim 30^{\circ}$  [7].

The large room for diversity in the profile, dimension, and installation of PBCFs for the best possible gain in energy efficiency has spurred interest in PBCF research. Table 1 summarizes the representative investigations in the past years, including model- and full-scale tests [7], numerical analysis [8,9], numerical study with model-scale tests [10–12], and model-scale tests [13]. Here, two issues need to be mentioned. First, the information is incomplete because some parameters or ranges are not explicitly stated in the relevant literature. Second, all the parameters or terms in the table are elaborated in detail later, combined with illustrations or equations. The results or findings in different references may be inconsistent, which can be understood since PBCFs are typically designed for a particular propeller system. In general, implementation of PBCFs is more effective on an old propeller than on a modern propeller.

Table 1. The PBCF dimensions and installation—the parameters and ranges chosen by different researchers.

Authors	Propeller Advance Ratio $J$	Boss Cap: Slope Angle $\varphi$	PBCFs Dimension: Diameter $D_{PBCF}$ , Chord Length $l_c$ , Camber $c$	PBCFs Installation Circumferential Position $a$ , Axial Position $b$ , Installation Angle $\alpha$ , Rake Angle $\theta$ , Phase Angle $\gamma$	Propeller Efficiency Gain
Ouchi et al. [7]	0~1.1		$D_{PBCF} = 0.09 \sim 0.175D_p$ $l_c = 0.09D_p, 0.12D_p$	$a < 0.07D_p, b = 0 \sim 0.08D_p$ $\alpha = 45 \sim 105^{\circ}, \theta = \pm 30^{\circ}$	$\leq 7\%$
Hsin et al. [8]			$D_{PBCF} = 0.2 \sim 0.25D_p$	$b < 0.025D_p$	1.4~1.6%
Ghassemi et al. [9]		0~15°	$D_{PBCF} = 0.33D_p$		Increase
Lim et al. [10]	0~1.0	-12°~-6°	$D_{PBCF} = 0.28 \sim 0.31D_p$	$\alpha = 61.5 \sim 71.5^{\circ}, \theta = \pm 10^{\circ}$	1.4~2%
Seo et al. [13]	0.1~0.9		$l_c = 0.078 \sim 0.14D_p$	$\alpha = 32 \sim 56^{\circ}, \gamma = 0 \sim 60^{\circ}$	1.6%
Mizzi et al. [11]			$l_c = 0.053 \sim 0.11D_p$	$\alpha = \pm 50^{\circ}, \gamma = 0 \sim 71^{\circ}$	1.3%
Gaggero [12]	0.4~1.1		$D_{PBCF} = 0.25 \sim 0.45D_p$ $l_c = 0.07 \sim 0.15D_p$ $c = -0.015 \sim 0D_p$	$b = 0.05 \sim 0.2D_p$ $\alpha = 30 \sim 60^{\circ}$ $\gamma = -45 \sim 40^{\circ}$	0.9, 4.0%

This paper presents our optimum design of PBCFs for a modern four-blade controllable pitch propeller attached to a Ro-Ro ship. The propeller has a diameter of 4.8 m and has

no fin on its boss cap in the original design. First, the experiment was performed on a down-scaled propeller/rudder system and a CFD model was developed to accurately reproduce the experiment. Then, the validated CFD model was deployed to perform the optimum design of PBCFs for the down-scaled propeller/rudder system. Ten different fin profiles, including the rectangle fin commonly used as PBCFs, and nine airfoils with good potential for being used as PBCFs, were numerically assessed for their impacts on the propeller/rudder system when they are used as the PBCFs. NACA4412 was found to be the best performing profile in terms of energy efficiency gains. Therefore, NACA4412 was selected as the fin profile for further optimum design of the PBCFs. The performance and flow characteristics of the propeller/rudder system with the new and optimized PBCFs were compared against the original system under both design and off-design operating conditions, showing consistently good energy efficiency gains. To implement the optimized PBCFs onto the real propeller, a yield strength analysis was finally performed, which shows that this is a feasible optimum design.

## 2. Methodology

### 2.1. Experimental Tests on a Model-Scale Propeller/Rudder System

The original propeller is a modern four-bladed controllable pitch propeller without fins on its boss cap. For a complete description of the propeller, many parameters are needed, in which the diameter and blade pitch angle are essential for a proper design of PBCFs. The propeller has a diameter of  $D_p = 2R_p = 4.8$  m. The propeller blade root profile is located at  $r_{p,br} = 0.281R_p$  and has a pitch of 5.6 m. The blade root pitch angle, defined as the angle between the rotation plane and profile chord, is determined as  $\varepsilon = \tan^{-1}\left(\frac{5.6}{2\pi r_{p,br}}\right) = 52.89^\circ$ . Though the propeller on the Ro-Ro ship is a controllable pitch propeller, it is analyzed in this study as a fixed pitch propeller with a constant blade root pitch angle of  $52.89^\circ$ . The propeller/rudder system is down-scaled by a factor of 21.24, resulting in a model-scale system on which all the work presented in this study is conducted. The model-scale propeller is shown in Figure 2. The main geometrical parameters are summarized in Table 2.

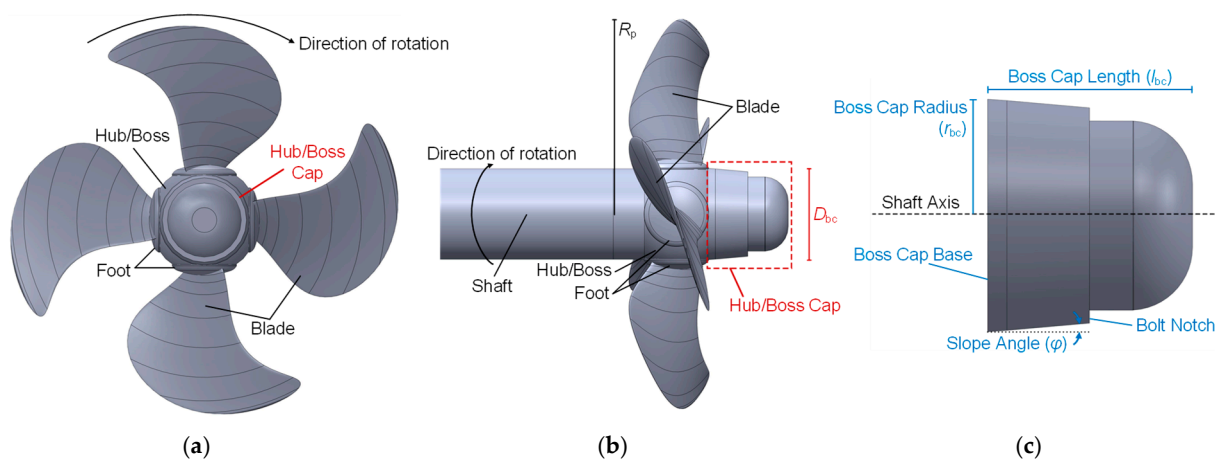


**Figure 2.** The model-scale propeller and propeller boss cap, in which  $R_p$  represents the radius of the propeller, and  $D_{bc}$ ,  $r_{bc}$ ,  $l_{bc}$ , and  $\varphi$  denote the diameter, radius, length, and slope angle of the boss cap, respectively. In this project, the slope angle  $\varphi < 0$ , i.e., a converging boss cap. (a) Frontal view of the propeller. (b) Side view of the propeller. (c) Side view of the boss cap.

**Table 2.** The model-scale modern propeller investigated in this paper.

Term	Propeller Diameter $D_p (=2R_p)$	Blade Root Pitch Angle $\varepsilon$	Boss cap Base Diameter $D_{bc} (=2R_{bc})$	Boss Cap Length $l_{bc}$	Blade Root Radius $r_{p,br} (=0.281R_p)$
Value	226 mm	$52.89^\circ$	53.02 mm	46.74 mm	31.75 mm

First, open water tests were conducted for the model-scale propeller/rudder in the large towing tank of the Hamburg Ship Model Basin with a length of 300 m, width of 18 m, and depth of 5.6 m. Self-propulsion tests were conducted on the down-scaled hull model including all appendages such as propellers, rudders, brackets, and thrusters in calm water with fixed ship motion. Each test run was made to reach self-propelled equilibrium of longitudinal forces between the ship resistance, propeller thrust, and external towing force by adjusting propeller rotational velocity at a constant towing speed. The external towing force was applied along the line of the propeller shaft for taking into account the difference in the hull surface friction coefficients between the model and full scales. The towing speed (i.e., ship speed  $V_A$ ) and propeller rotational velocity  $\omega$  were varied to keep the similar advance ratio  $J$ , and the corresponding thrust and torque values were measured. From them, the thrust coefficient  $K_T$ , torque coefficient  $K_Q$ , and propeller efficiency  $\eta_o$  were determined. One of the advantages of open water tests is the elimination of cavitation effects. Commonly used ship propeller terminology is introduced below.

$$J = \frac{V_A}{\omega D_p} \quad (1)$$

$$K_T = \frac{T}{\rho_\infty (\omega D_p)^2 \cdot D_p^2} \quad (2)$$

$$K_Q = \frac{Q}{\rho_\infty (\omega D_p)^2 \cdot D_p^3} \quad (3)$$

$$\eta_o = \frac{J K_T}{2\pi K_Q} = \frac{V_A T}{2\pi\omega Q} \quad (4)$$

$$C_p = \frac{p - p_\infty}{\frac{1}{2} \rho_\infty (\omega D_p)^2} \quad (5)$$

where  $J$ ,  $V_A$ ,  $\omega$ ,  $D_p$ ,  $K_T$ ,  $T$ ,  $\rho_\infty$ ,  $K_Q$ ,  $Q$ ,  $\eta_o$ ,  $C_p$ ,  $p$ , and  $p_\infty$  represent the advance ratio, ship speed, propeller rotational velocity, propeller diameter, thrust coefficient, thrust, density of freestream flow, torque coefficient, torque, propeller or propulsive efficiency, pressure coefficient, pressure, and pressure of freestream flow, respectively.

## 2.2. Development of a Digital Twin to Reproduce the Experiment

Then, a CFD model was developed to numerically reproduce the experiment, using our experience in this area [14,15]. A cylindrical computational domain with a radius of  $4D_p$  was defined, as shown in Figure 3. The computational domain extends  $3D_p$  and  $6D_p$  upstream and downstream of the propeller reference line, respectively. The left, right, and side of the cylindrical domain are defined as a velocity inlet, pressure outlet, and wall with slip, respectively, to replicate the open water condition in the tests. The zoom-in of the rotational cylindrical subdomain around the propeller is also shown in Figure 3.

Since all the stationary boundaries with respect to the inertial frame are surfaces of revolution about the axis of rotation, a single moving reference frame (MRF) was used in the CFD study [11,12] to render the problem, which is instability in the inertial frame, steady with respect to the moving frame. As a preliminary sensitivity study, both the MRF and sliding mesh method were used and compared in a simulation of a base case. The computationally expensive sliding mesh method was expected to better estimate the hub vortex evolution and describe how the PBCFs mitigate the hub vortex. Our simulation shows that the two methods yielded very similar results in the thrust coefficient, torque coefficient, and propeller efficiency, which is the main concern of this study. As a result, the computationally efficient MRF method was finally used in the study. As shown in Figure 3, an MRF subdomain surrounding the propeller was defined, on which a rotational velocity was specified. The equations of fluid dynamics defined with respect to the MRF needed to be modified accordingly. For this problem in which the MRF has a constant rotation

and zero translation, the Coriolis acceleration due to the rotation of the frame and the centripetal acceleration due to the fluid motion in a uniform circular path were accounted for and treated as source terms in the modified momentum equations.

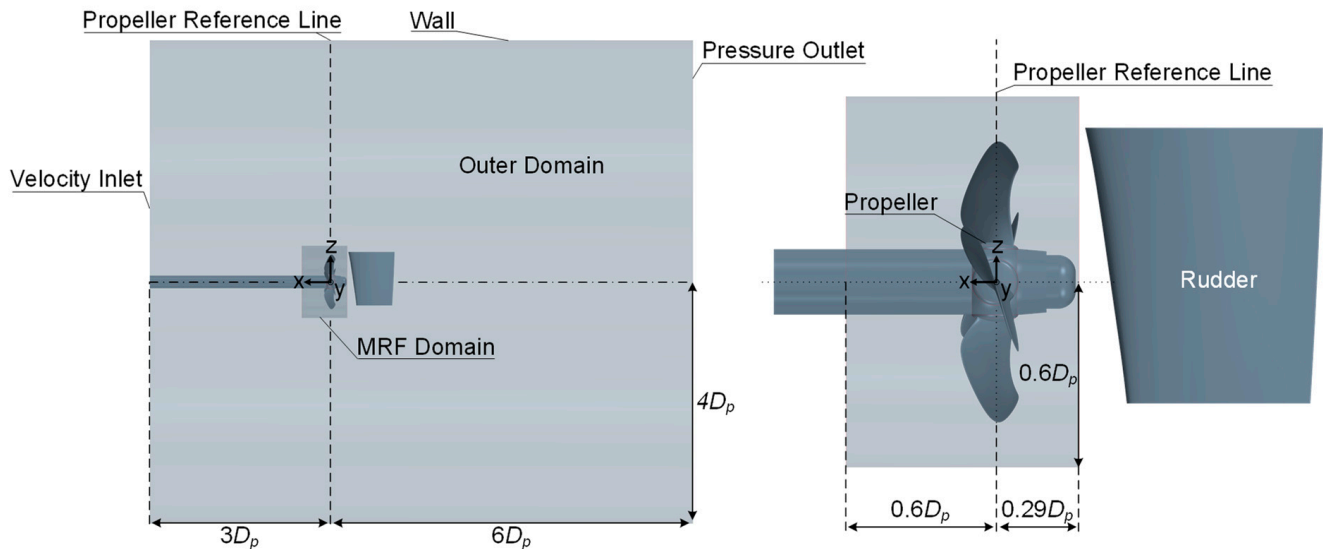


**Figure 3.** The entire computational domain (left); the zoom-in of MRF domain and rudder (right).

For the propeller flows, the transition from laminar to turbulent boundary layer can strongly influence flow blockage and boundary layer separation. To properly account for this effect, the transition SST  $k - \omega$  model was employed, which is based on the coupling of the SST  $k - \omega$  model with two other transport equations. One is for the intermittency  $\gamma$ . The other is for the transition onset criterion in terms of momentum–thickness; Reynolds number  $Re_\theta$ . SST  $k - \omega$  model is commonly used in the relevant literature, e.g., [11,12]. However, as discussed in [11], the accuracy of the simulation results can be improved by employing a transition model, especially for model-scale propellers in which the transition behavior within the boundary layer is more significant than that for full-scale propellers. As a result, the transition SST  $k - \omega$  model was used with the all- $y^+$  wall treatment in this study.

The computational domain is carefully meshed in both mesh quality and mesh density, especially in the near-wall region. To perform a grid convergence index (GCI) analysis, three different meshes with  $2.20 \times 10^5$ ,  $1.75 \times 10^6$ , and  $1.41 \times 10^7$  cells, respectively, were created for the experimental cases in which the original model propeller without PBCFs was tested. Due to the complexity of the geometry, all three were unstructured meshes in overall, but with the fine and structured boundary layer meshing in the near-wall region. The average  $y^+$  on the walls in the MRF domain was 3.12, 0.41, and 0.39 for the coarse, medium, and fine mesh, respectively. Based on the three meshes, the key simulation results were compared and a GCI analysis was conducted. The mesh finally used in numerically reproducing the experimental cases and the corresponding GCI analysis results is summarized in Table 3. The detailed procedure for a GCI analysis in CFD applications can be seen in [16]. The low relative error and extrapolated relative error in the GCI study indicate that the fine mesh is expected to generate practically grid-independent simulation results. The GCI = 1.9% and 0.2% means that based on the fine mesh, the numerical error in the solution of the thrust coefficient  $K_T$  and the torque coefficient  $K_Q$  is estimated to be 1.9% and 0.2%, respectively. This is very good for a CFD study. As seen in Table 3, the fine mesh has an average  $y^+ = 0.39$  on the wall surfaces in the MRF domain, which is important for correctly predicting the forces on the propeller and the performance of the propeller system. The meshes used in the subsequent simulations for screening the appropriate fin profiles and for optimizing the PBCFs were developed from the fine mesh here, with the similar average  $y^+$  on both the blades and fins. The total number of cells depends on the shape and size of the PBCFs, slightly above  $1.41 \times 10^7$  in all the computational cases with PBCFs. The CFD

simulation was performed using STAR-CCM+. To ensure that the simulations are well-converged, both the scaled residuals and the thrust and torque of the blade are monitored during the iterations. After ca. 600–1000 iterations, the scaled residuals in all the governing equations reduce and stabilize below  $10^{-3}$ , and both the thrust and torque converge to constant values.

**Table 3.** The fine mesh used in a base simulation and the grid convergence index (GCI) based on the thrust and torque.

The Mesh Finally Used in Reproducing the Experimental Cases after a GCI Study: Terms vs. Values		
Number of cells	1.41 × 10 <sup>7</sup> (1.15 × 10 <sup>7</sup> in MRF domain)	
$y^+$ on walls in the MRF domain	0.39 in average (in range of 0.02 – 1.7)	
Skewness angle between vector connecting two cell-centers and face normal	1.1° in average (maximum of 88.5°)	
Cell volume ratio—the ratio of the volume of a cell to its largest neighbor	0.98 in average (minimum of 0.0001)	
GCI Based on the Thrust Coefficient $K_T$ and Torque Coefficient $K_Q$ for the Mesh Summarized above		
	$K_T$	$K_Q$
Relative error, $e_a$	3.8%	1.4%
Extrapolated relative error, $e_{ext}$	1.5%	0.1%
Grid convergence index, GCI	1.9%	0.2%

### 2.3. CFD-Based Screening of Appropriate Fin Profile for PBCFs Design

After being validated against the experiment, the CFD model was deployed to screen the appropriate fin profile for the PBCFs' design. To facilitate the installation of the PBCFs, the original propeller boss cap in Figure 2c was slightly redesigned, in which the practical manufacturing issues such as the slope angle and internal bolting limitation were all considered. The new propeller boss cap in Figure 4a has the same length and base diameter as the original one. The CFD model was used to evaluate the impact of the new boss cap on the performance of the propeller/rudder system, which shows a slight efficiency increase of 0.17% over the original propeller/rudder system mainly due to the more streamlined boss cap design. The new boss cap was found to have an insignificant impact on the hub vortex.

Our comprehensive literature study shows that the overwhelming majority of PBCFs are based on the rectangular fin profile, e.g., as proposed in the first patent for PBCFs [17], and airfoils are rarely used as PBCFs. On the other hand, airfoils have been widely used in the maritime industry. For example, the cross-sections of modern propellers and rudders are constructed from the basis of airfoils. In our study, nine airfoils with good potential for being used as PBCFs profiles were chosen, mainly based on their lift-to-drag ratio  $C_L/C_D$  (i.e., the amount of lift generated by an airfoil, compared to its drag which is a resistance). It must be emphasized that the selection of these airfoils was rational. The higher the lift-to-drag ratio  $C_L/C_D$  is, the higher the lift and efficiency tend to be. Table 4 summarizes all the 10 profiles, in which the maximum  $C_L/C_D$  of the airfoils and the corresponding angle of attack (AoA) are from Airfoil Tools [18]. The maximum  $C_L/C_D$  is evaluated at a Reynolds number of  $Re = \frac{V_s l_c}{\nu_\infty} = \frac{2.08 \text{ m/s} \times 0.027 \text{ m}}{1.191 \times 10^{-6} \text{ m}^2/\text{s}} \approx 5 \times 10^4$  and a critical number of  $N_{crit} = 5$ . This critical number, depending on the free flow turbulence, is used to simulate the laminar-to-turbulent boundary layer transition point when no forced transition trip locations are specified for the top and bottom surfaces of an airfoil. The airfoil profile CH10 was investigated due to its high lift at low Reynolds numbers, despite its high drag. Airfoil NACA4412, as shown in Figure 4b, has been widely used for nearly a century.

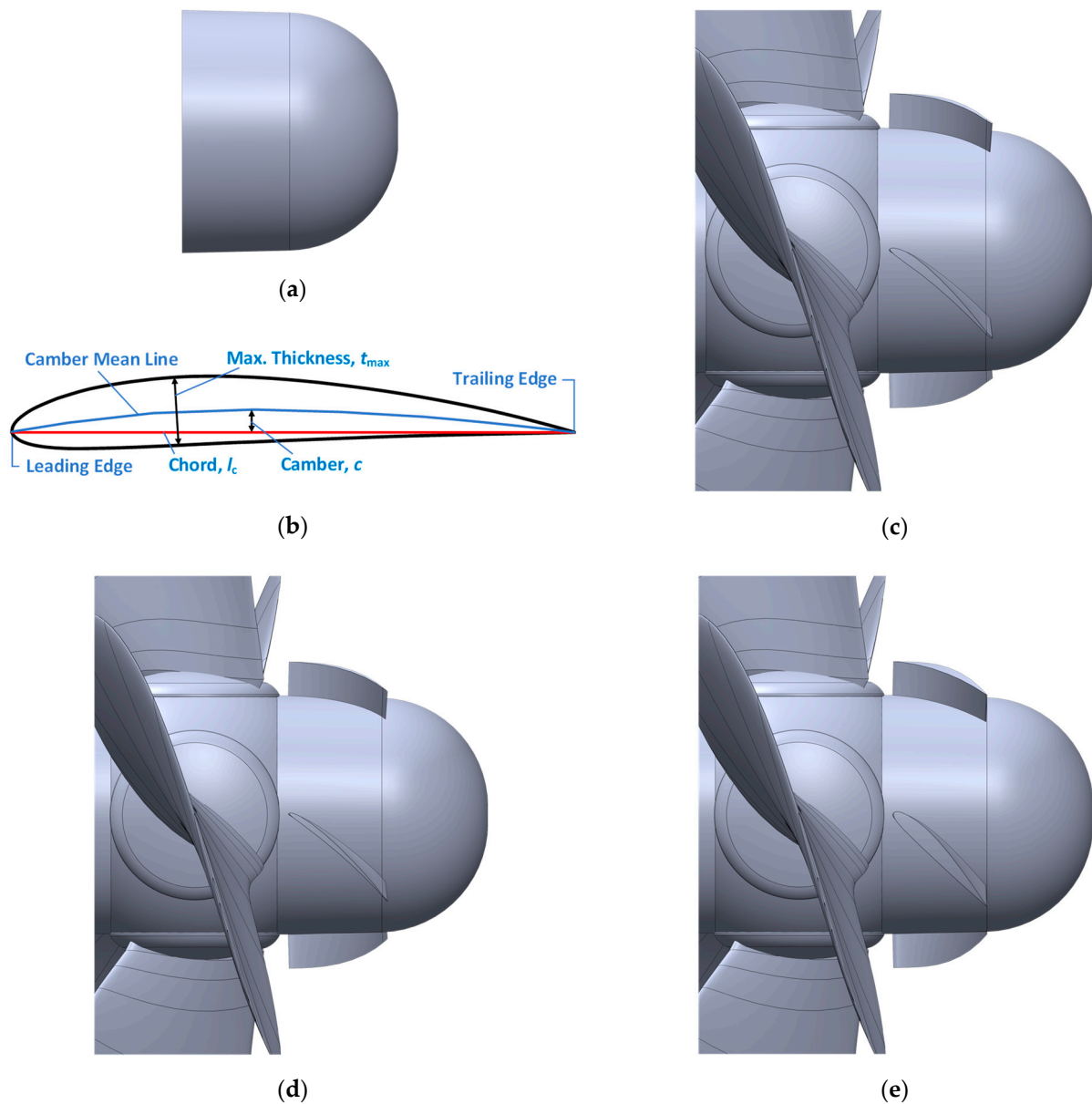


**Figure 4.** New boss cap and propeller with base design of representative airfoil PBCFs. (a) New boss cap facilitating fin installation. (b) Airfoil—terminology and dimension. (c) Base design of PBCFs of profile 1, AH-6-40-7. (d) Base design of PBCFs of profile 4, E63. (e) Base design of PBCFs of profile 6, NACA4412.

**Table 4.** Ten boss cap fin profiles: their max lift/drag ratio and angle of attack (AoA, i.e., the angle between flow direction and chord line), and their installation angles finally used in our base design.

Profile no.	0	1	2	3	4	5	6	7	8	9
Profile Name	Rectangle	AH-6-40-7	Bergey BW-3	CH10	E63	GOE79	NACA4412	Cp-100-050-gn	20-32C	S1223
Max $C_L/C_D$	–	46.9	46	12.4	51.1	42.7	36.1	23.9	40.8	42.3
AoA for max $C_L/C_D$	–	4.8°	5.0°	3.5°	5.3°	5.5°	8.5°	11.0°	3.8°	3.3°
Our base design: Installation angle $\alpha$	51.5°	53.4°	53.1°	54.6°	52.9°	52.6°	49.6°	47.1°	54.4°	54.9°

To compare the performance and evaluate the potential of the 10 profiles as the PBCFs, a literature study was performed first, from which the preferable dimensions and installations in the PBCFs' design, with respect to the propeller diameter  $D_p$  and propeller blade root pitch angle  $\varepsilon$ , are given in Table 5. The key terminology, dimension,

and installation parameters of the PBCFs are visually indicated in Figure 5. In the table and figure,  $R_p$  and  $r_{PBCF}$  represent the radius of the propeller and the PBCFs, both from the shaft axis to the tip.  $l_c$ ,  $t$ , and  $s$  denote the fin chord length from the leading edge to the trailing edge, fin thickness, and fin span height from the boss cap surface to fin tip, respectively.  $a$  and  $b$  are the circumferential and axial distance of the fin leading edge, indicating the fin installation position.  $\alpha$  is the installation angle between the fin chord and the fin installation plane which is perpendicular to the shaft axis, and is also referred to as the fin root pitch angle.  $\varepsilon$  represents the propeller blade root pitch angle. It needs to be mentioned that the rake or inclination angle  $\theta$  of the PBCFs, inclined against ( $\theta > 0$ ) or towards ( $\theta < 0$ ) the rotation direction, or normal ( $\theta = 0$ ) to the boss cap surface curvature, was found to have an insignificant impact on the performance of the propeller compared to others such as PBCF diameter and installation position [10,17].

**Table 5.** Preferable design of PBCFs recommended in the literature vs. Our base design of the PBCFs.

Term	Boss Cap	Number of Fins	Profile of Fins	Diameter of Fin, $D_{PBCF}$	Chord of Fin, $l_c$	Thickness of Fin, $t$	Installation Angle, $\alpha$	Installation Position, $a, b$	Rake Angle, $\theta$
Preferable design	Converging	Same as blades	Rectangle or airfoil	$D_{PBCF}/D_p \leq 0.30$	$l_c/D_p \leq 0.12$	$t/D_p \approx 0.005$	$-5^\circ \leq \alpha - \varepsilon \leq 5^\circ$	$a/D_p \leq 0.070$ $b/D_p \leq 0.075$	$-30^\circ \leq \theta \leq 10^\circ$
Our base design	Converging	$n = 4$	10 profiles	$D_{PBCF}/D_p = 0.296$	$l_c/D_p = 0.12$	$t/D_p = 0.0045$	See Table 4	$a/D_p = 0.044$ $b/D_p = 0.031$	$\theta = 0^\circ$

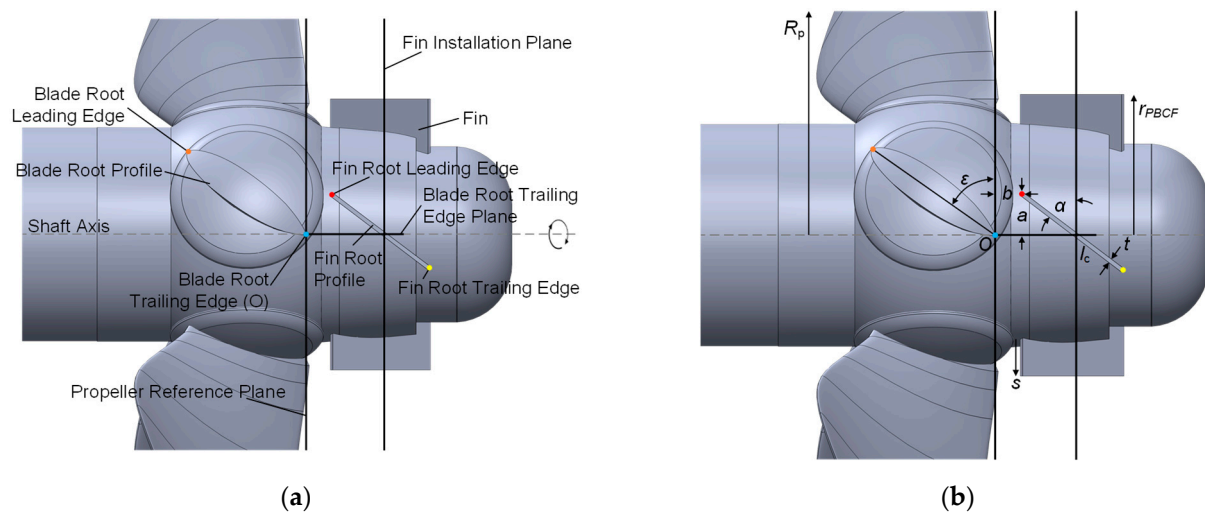


**Figure 5.** The model-scale propeller with rectangular PBCFs, in which all the key terminologies and design parameters are visually indicated. (a) Definition of profiles, axes, planes, and points. (b) Key PBCFs sizing and installation parameters.

By following the preferable design in Table 5, we conducted and compared the base design of the 10 PBCFs for the model-scale propeller ( $D_p = 226$  mm and  $\varepsilon = 52.89^\circ$ ). All the dimension and installation parameters, except the installation angle, are also given in Table 5, directly in parallel with the recommended design range in the literature.

The installation angles are given in Table 4. For the rectangle PBCFs, the installation angle was determined to be  $\alpha = 51.5^\circ$ , which was calculated directly from  $\alpha - \varepsilon = -1.4^\circ$ . For the airfoil-based PBCFs, the optimum installation angle  $\alpha$  depended on both the propeller blade root pitch angle  $\varepsilon$  and the angle of attack (AoA) and was determined from a preliminary simulation-based sensitivity study. As seen in Table 4, the installation angles finally used in the base design are in the preferable range of the installation angle,  $47.89^\circ = \varepsilon - 5^\circ \leq \alpha \leq \varepsilon + 5^\circ = 57.89^\circ$ , except profile 7 (Cp-100-050-gn) for which the installation angle  $\alpha = 47.1^\circ$  is slightly out of the range. To gain a visual understanding of the base design, the propellers with the representative PBCFs based on the airfoil profile 1 (AH-6-40-7), 4 (E63) and 6 (NACA4412) are shown in Figure 4c–e, respectively.

To evaluate which profile can be best used as the PBCFs for the model-scale propeller/rudder system, two sets of CFD simulations were conducted for the base design:

one under the same design operating condition, and one under the same thrust. From the comparison, the best performing fin profile can be determined.

#### 2.4. CFD-Based Optimization Design of the PBCFs Using the Best Performing Fin Profile

Finally, a comprehensive CFD-based parametric study and optimization was performed for the best performing fin profile, resulting in the optimum design of the PBCFs. Mathematically, the target of the optimization was to maximize the propeller efficiency  $\eta_o$ , with the main constraints being the existing propeller/rudder geometry and dimensions. Physically, the optimization of the PBCFs was to minimize the hub vortex as much as possible and to increase the thrust. The performance of the propeller/rudder system with the new optimized PBCFs was assessed under both design and off-design operating conditions. A yield strength analysis was also performed, assuring that the optimum design of the PBCFs is practicably feasible and can be manufactured and implemented in industrial vessels as a cost-effective energy-saving device.

### 3. Results and Discussion

#### 3.1. Experimental Validation of CFD for the Original Propeller/Rudder System without PBCFs

The thrust, torque, and efficiency obtained from the experiments were used to validate the CFD model. The derivation between the CFD results and experimental data under different test conditions are summarized in Table 6. The very good agreement between the CFD and experiments over the entire test range of ship velocity also justifies the use of the transition SST  $k - \omega$  model. As the ship speed or advance ratio increases, the transition from laminar boundary layer to turbulent boundary layer becomes increasingly important. Neglecting the transition in turbulence modeling can induce high deviation from the experimental data. To avoid repetition, the detailed CFD results of the original model-scale propeller/rudder system, which were used to benchmark the performance of the propeller/rudder system with new optimized PBCFs, are presented later.

**Table 6.** Validation of CFD with testing results for the original model-scale propeller/rudder system.

Ship (or Water Inflow) Speed, $V_S$ [m/s]	2.02	2.08	2.13	2.19	2.25	2.30	2.36	2.42	2.47
Deviation in thrust coef., $\frac{(K_{T,CFD} - K_{T,exp}) \times 100}{K_{T,exp}}$ [%]	0.6	0.7	1.0	1.4	1.3	1.5	1.8	1.7	1.9
Deviation in torque coef., $\frac{(K_{Q,CFD} - K_{Q,exp}) \times 100}{K_{Q,exp}}$ [%]	1.1	1.2	1.5	1.8	1.8	1.9	2.1	2.1	2.3
Deviation in propeller eff., $\frac{(\eta_{o,CFD} - \eta_{o,exp}) \times 100}{\eta_{o,exp}}$ [%]	-0.5	-0.5	-0.5	-0.4	-0.5	-0.4	-0.4	-0.4	-0.3

#### 3.2. CFD-Based Screening of the Best Performing Fin Profile for PBCF Design

For each fin profile, the improvement of efficiency over the original propeller without PBCFs,  $\Delta\eta_o / \eta_o$ , are shown in Figure 6. Under the same advance ratio and rotational speed, airfoil profiles 1 (AH-6-40-7), 4 (E63), and 6 (NACA4412) obviously outperformed the rectangular fin in terms of efficiency improvement. However, the efficiency gain could be partly induced by the increased thrust. To better compare the propeller with PBCFs against the original propeller as well as cross compare the different PBCFs, one needs to maintain the same thrust, which is achieved by adjusting the rotational speed of the propeller and, thus, adjusting the forward motion of the propeller. In the simulation, we used a proportional controller to retain the thrust as close to the original propeller as possible. The updated improvement of efficiency showed the same trend, as seen in Figure 6. Airfoil profiles 1, 4, and 6 were still the three best performing PBCFs, in which profile 6 (NACA 4412) stood out as the best under the optimal installation angle of  $\alpha = 52^\circ$ . A further inspection of the thrust and torque coefficients shows that profile 6 achieved the best thrust coefficient before implementing the thrust controller, which lowered the rotational speed of profile 6 to a larger extent than other profiles and, thus, improved the efficiency.

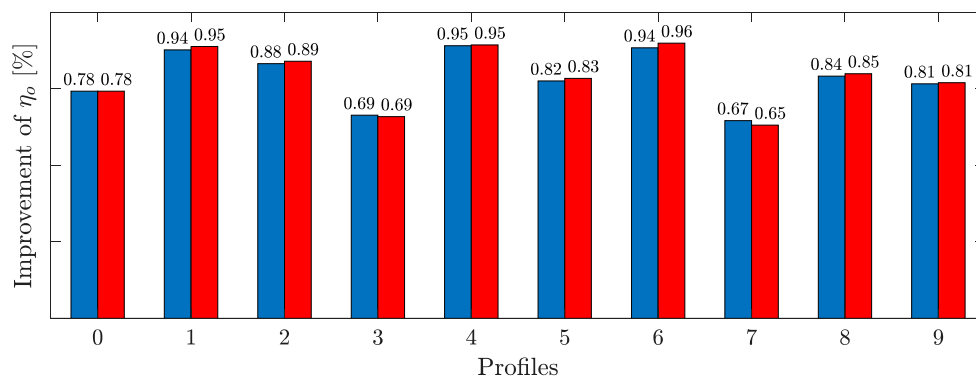


**Figure 6.** Propeller efficiency increase ( $\Delta\eta_0/\eta_0$ ) by implementing different profiles as the PBCFs in the base design: under the same advance ratio and rotational speed (blue bar, on the left in each pair) and under the same thrust (red bar, on the right in each pair).

This is in good alignment with the recent study [19], in which four airfoil-based PBCFs were numerically investigated for their impacts on the performance of a model five-blade propeller in open water conditions and NACA4412 airfoil-based PBCFs were found to have the greatest effect on the propeller efficiency.

### 3.3. CFD-Based Optimum Design of the PBCFs

NACA4412 (i.e., profile 6) was finally used in the optimum design of the PBCFs. Besides the optimal number of fins ( $n = 4$ ) and installation angle ( $\alpha = 52^\circ$ ), the other dimension and installation parameters in Table 5, as well as the shape or profile of NACA4412, were further investigated for their impacts on the performance of the propeller/rudder system.

To better understand NACA4412 shape optimization, the terminology of the four-digit NACA airfoils will be briefly introduced. The first digit expresses the maximum camber in percent chord, the second digit defines the location of the maximum camber point in tenths of the chord, and the last two digits gives the maximum thickness in percent chord. Thus, 4412 has a maximum camber of 4% of the chord located at 40% chord from the leading edge and has a maximum thickness of 12% of the chord.

Figure 7 shows the effects of the key PBCFs dimension, shape, and installation parameters on the efficiency gains of the model-scale propeller/rudder system under the design operating condition. The propeller under study has a diameter of  $D_p = 226 \text{ mm}$ , a blade root pitch angle of  $\varepsilon = 52.89^\circ$ , and a boss cap base diameter of  $D_{bc} = 53.02 \text{ mm}$ .

The PBCFs' span height shows a great impact on the propeller efficiency. As a result, much attention needs to be paid to the span height (or the diameter) of the PBCFs. For our model propeller, a span height of  $s = 7.5 \text{ mm}$  yielded the highest efficiency, corresponding to a PBCFs-to-propeller diameter ratio of  $D_{PBCF}/D_p = 0.3$ . It is in the recommended range of  $D_{PBCF}/D_p$  despite being above the stated optimum in the literature [12,17]. This is mainly because the boss cap utilized in our project has a larger diameter, with a boss ratio of  $D_{bc}/D_p = 53.02/226 = 0.23$ , whereas a boss ratio of 0.18 is applied in the literature. The boss cap of a larger diameter makes the PBCFs' root placement farther away from the shaft axis. As the span height increases in the range of  $3 \leq s \leq 13 \text{ mm}$ , the thrust coefficient first increases and then decreases and the torque coefficient decreases monotonically, yielding the highest efficiency at a span height of  $s = 7.5 \text{ mm}$ . Compared to the span height, the chord length showed a less pronounced impact on the efficiency. Figure 7 indicates that a chord length of  $l_c = 30 \text{ mm}$  yielded the highest propeller efficiency. It is equivalent to a chord length of  $l_c = 0.13 D_p$ , which also aligns with the recommendation for PBCF design [12,17]. Since the chord length indirectly affects the propeller efficiency via NACA airfoil shape optimization (e.g., maximum camber and its position, maximum thickness), it is still considered an important parameter in PBCF design.

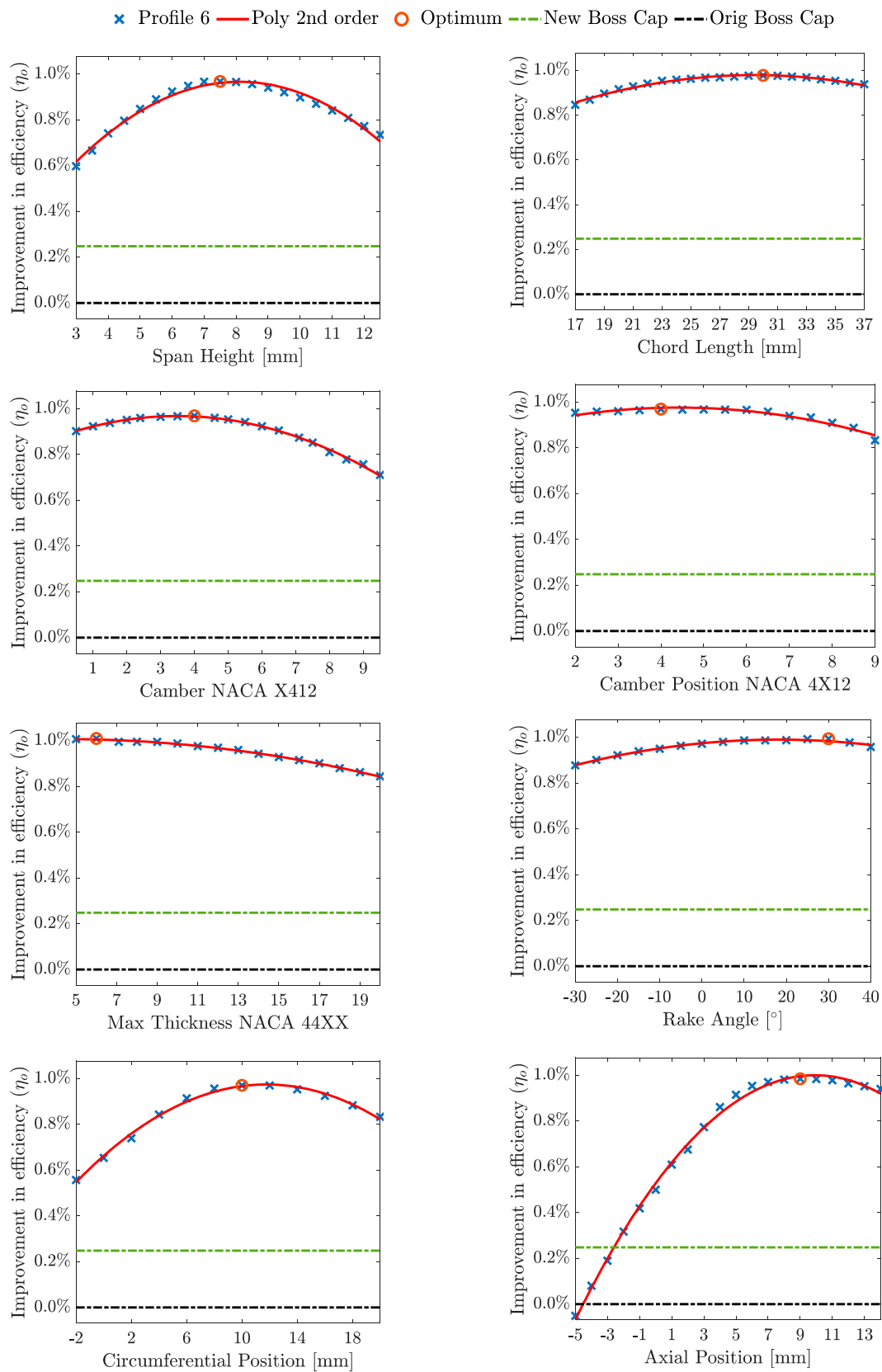


**Figure 7.** Effects of the overall NACA4412 airfoil fin dimension (span height, chord length), airfoil shape (maximum chamber X412 and its position 4X12, maximum thickness 44XX), and fin installation (rake angle, circumferential, and axial position) on the efficiency improvement of the propeller/rudder system.

Optimization of the NACA4412 airfoil profile was also performed. The maximum camber  $X = 4$  in X412, i.e., the maximum camber  $c = 4\% \cdot l_c$ , yielded the largest efficiency gain, as seen in Figure 7. Similarly, the position of the maximum camber  $X = 4$  in 4X12, i.e., the maximum camber located at  $4 \cdot 10\% \cdot l_c$  from the leading edge, resulted in the largest efficiency improvement. The latter showed a much less pronounced impact on the efficiency than the former. Compared to the two parameters, the maximum thickness showed a different trend in efficiency improvement. As the maximum thickness decreased in the range of investigation (i.e.,  $XX = 05\text{--}20$  in 44XX), the efficiency increased monotonically. The lower limits of the maximum airfoil thickness, e.g.,  $XX = 04, 03, 02,$  or  $01$ , were not investigated, since too thin fins may fail due to stresses or fatigue.  $XX = 05$ , i.e., maximum thickness being 5% of the chord length ( $t_{max} = 5\% \cdot l_c$ ), was equivalent to  $t_{max} \approx 0.01R_p$  in our study, which is close to what was used in [17]. In our optimum design, the maximum thickness of  $XX = 06$  in 44XX was used, which means that the maximum airfoil thickness  $t_{max}$  equals to 6% of the chord length  $l_c$ . Compared to  $t_{max} = 5\% \cdot l_c$ , the maximum thickness of  $t_{max} = 6\% \cdot l_c$  yielded almost the same efficiency but improved the robustness. A yield strength analysis will be performed later to further examine if the PBCFs of a maximum thickness of  $6\% \cdot l_c$  can withstand practical operation.

Besides the overall PBCFs dimension and NACA4412 airfoil shape, the PBCFs' installation was optimized for the highest possible efficiency gain. The impact of the rake angle is inconclusive in the literature. For example, an optimum rake angle of  $\theta = -30^\circ$  was found among  $30^\circ, 0^\circ,$  and  $-30^\circ$  in [7], whilst the rake angle was concluded to be insignificant and no clear tendency was observed for the three angles ( $10^\circ, 0^\circ,$  and  $-10^\circ$ ) in [10]. In our study, an optimum rake angle of  $\theta = 30^\circ$  can be seen in Figure 7, i.e., fins not perpendicular to the boss cap surface curvature but  $30^\circ$  inclined towards the direction of rotation. As the rake angle increased in the range of investigation, the thrust coefficient increased slightly, while the torque coefficient first decreased slowly and then increased slowly. Compared to other installation parameters such as installation angle and circumferential and axial positions, the impact of the rake angle on the propeller efficiency was much less pronounced and can be considered insignificant. Regarding the circumferential position  $a$ , Figure 7 shows that it has a significant influence on the efficiency, which is consistent with the findings in [9]. The optimum circumferential position  $a = 10$  mm (i.e.,  $a = 0.044 D_p$ ) yielded the highest efficiency gain for the propeller/ rudder system under study. This is in good alignment with the requirement on the circumferential position,  $a < 0.07 D_p$ , as proposed in the patent [17]. The axial position  $b$  also has a great impact on the propeller efficiency. Hsin et al. suggested the axial position should be located near the trailing edge of the propeller blade root and the axial position of  $b = 0.05 D_p$  may be the optimum [8]. Ogura et al. stated in their patent that the axial distance should be kept  $b < 0.075 D_p$  [17]. In our study, a wide range of the axial position,  $-5 \leq b \leq 14$  mm, was investigated. The lower end of this range was included to assess whether the leading edge of the PBCFs could better interact with the slipstreams or not, since the main slipstreams are close to the trailing edge of the propeller blades. However, as observed in Figure 7, it had only a negative effect. As the axial position decreased from  $b = 3$  mm to  $-5$  mm, the thrust coefficient decreased slightly and the torque coefficient increased rapidly, which lowered the efficiency compared to the original system. In the upper end of the range, there were only slight changes in both the thrust and torque coefficients, yielding relatively insignificant changes to the propeller efficiency. The axial position of  $b = 9$  mm was determined as the optimum point from the plot. It is equivalent to  $b = 0.035 D_p$ , which is in accordance with the literature.

A thorough understanding of the key design parameters of the PBCFs was achieved via the above parametric study, in which only one parameter was changed at a time and other parameters were retained at the values of the base design. To more appropriately account for the interactions between the key design parameters, the individual optimums were combined into CFD simulation, and minor adjustments were made and assessed. This resulted in the final optimum design of the PBCFs, as summarized in Table 7. To make the results beneficial for other propeller/rudder systems, the optimum design was generalized,

which is also presented in Table 7. Figure 8 shows the new propeller boss cap with the optimized PBCFs, together with the original boss cap for comparison.

**Table 7.** The optimum PBCF design for the model-scale propeller ( $D_p = 226$  mm,  $\varepsilon = 52.89^\circ$ ,  $D_{bc} = 53.02$  mm) vs. the derived general optimum PBCF design applicable to other propellers.

Design Parameter	Optimum Design	Generalized Optimum Design
Dimension		
Number of fins, $n$	4	$n =$ number of blades
Span height, $s \equiv \frac{D_{PBCF} - D_{bc}}{2}$ [mm]	7.5	$s = 0.033 D_p$ or $D_{PBCF} = 0.3 D_p$
Chord length, $l_c$ [mm]	30	$l_c = 0.13 D_p$
NACA profile		
Max. camber, $c$ [% of chord $l_c$ ]	4	–
Max. camber position [%·10 of chord from the leading edge]	4	–
Max. thickness [% of chord]	6	–
Installation		
Installation angle, $\alpha$ [ $^\circ$ ]	52	$\alpha - \varepsilon = -0.89^\circ$
Rake angle, $\theta$ [ $^\circ$ ]	30	$\theta - \varepsilon = -22.89^\circ$
Circumferential position, $a$ [mm]	10	$a = 0.044 D_p$
Axial position, $b$ [mm]	8	$b = 0.035 D_p$
Efficiency gain		
Percentage point	0.728	–
Percentage [%]	1.043	–



**Figure 8.** The original boss cap vs. the new boss cap with optimized fins. (a) Original boss cap. (b) New boss cap, with optimized PBCFs.

### 3.4. Performance of the Propeller/Rudder System with the New Optimized PBCFs

Figure 9 compares the pressure coefficient  $C_p$  contour on or around the original propeller/rudder and the propeller/rudder with the new optimized PBCFs under the design operating condition. The main difference lies in the downstream of the propeller boss cap. Implementation of the new optimized PBCFs cost-effectively weakens or eliminates the low-pressure zone induced by the hub vortex behind the propeller boss cap, reduces the drag and improves the propeller efficiency. Under the design operating condition, a propeller efficiency improvement of 0.728 percentage points or 1.043% over the original system was attained by the new optimized PBCFs. The streamlines were found to follow the fin profile at the leading edge, indicating that the installation angle of the PBCFs was properly optimized in our study. Figure 9b also shows the pressure profiles on both sides of a fin. As expected, on the pressure side, a zone of high pressure is observed at the fin's leading edge and on the boss cap, which needs to be minimized to further reduce the drag and, therefore, increase the efficiency. Recently, ducted PBCFs (i.e., PBCFs inside a nozzle)

were investigated as an attempt to mitigate possible side effects of conventional PBCFs, e.g., secondary vortical structures from the PBCFs tip, while not largely compromising the beneficial effects [20].

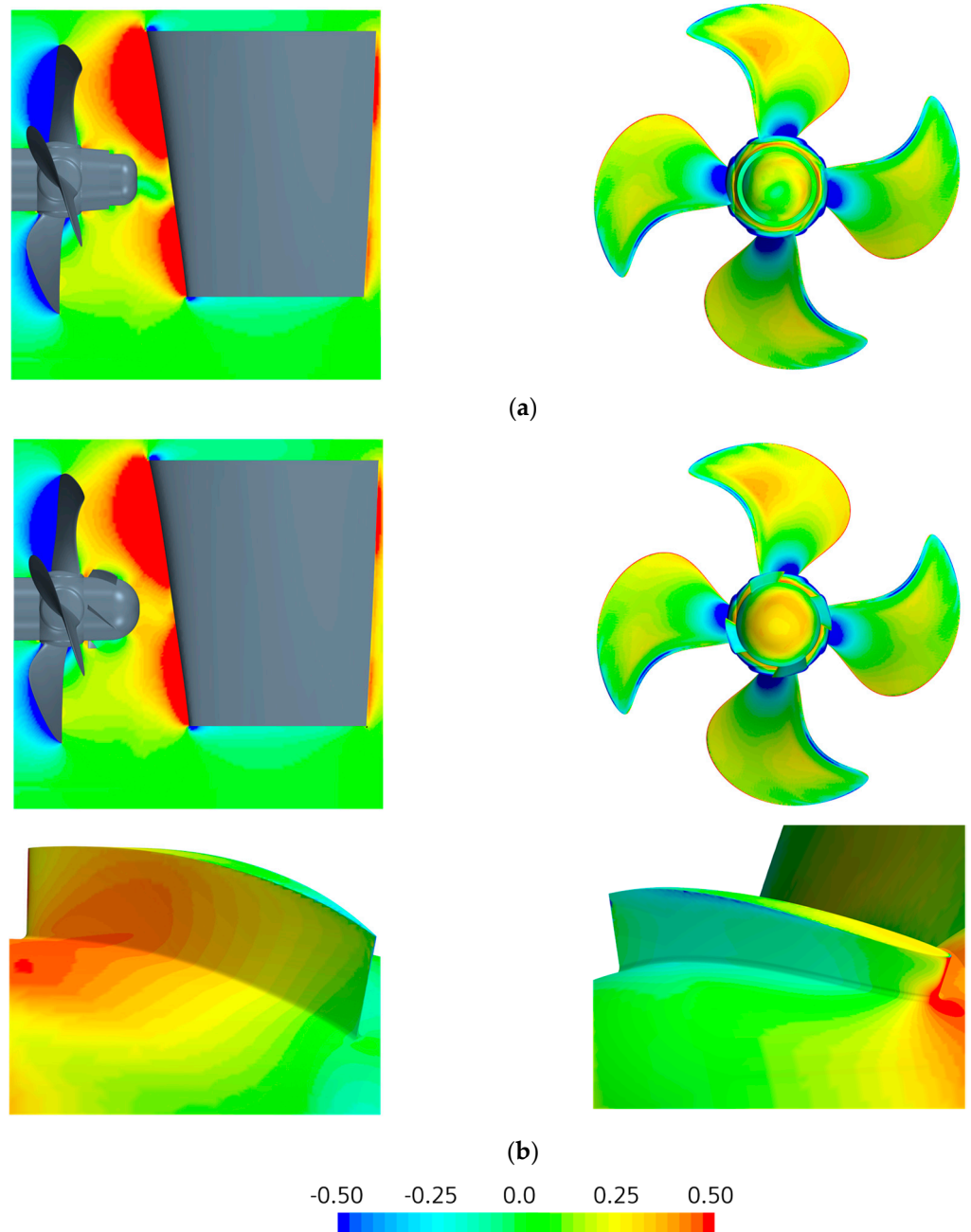
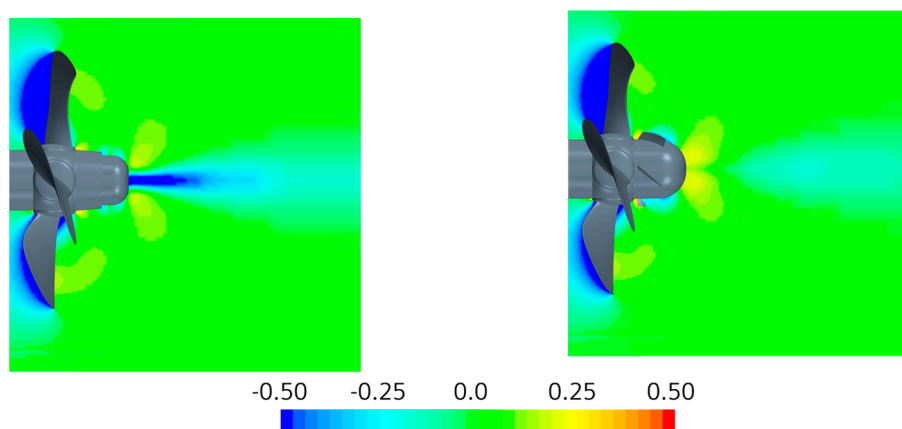


**Figure 9.** Pressure coefficient  $C_p$  on or around (a) the original propeller/rudder and (b) the new propeller/rudder with optimized PBCFs with the water flow of 2.25 m/s from the left to the right and rotational speed of 608 rpm. (a) Original propeller/rudder system: side view (left) and downstream view from the rudder (right). (b) Propeller/rudder system with new optimized PBCFs: side view (top left), downstream view from the rudder (top right), pressure side of a fin with the flow from left to right (bottom left), and suction side of a fin with the flow from right to left (bottom right).

To better visualize the impact of the optimized PBCFs on the hub vortex, simulations were performed for the original propeller and the propeller with the new PBCFs, both without the rudder. The pressure coefficients in Figure 10 clearly show that the PBCFs effectively eliminate the low-pressure zone induced by the hub vortex, reduce the drag and improve the efficiency. A zone of low pressure further downstream of the propeller boss

cap is still observed in the new system, which is insignificant since it does not compromise the PBCFs' performance.



(a) Original propeller without PBCFs (b) Propeller with new optimized PBCFs

**Figure 10.** Pressure coefficient  $C_p$  contour around the propeller without the rudder: (a) original propeller, (b) propeller with optimized PBCFs.

To further evaluate the performance of the propeller/rudder system with the new PBCFs, simulations were performed for different ship speeds in the range of 2–2.5 m/s with a step of 0.05 m/s. For the original propeller/rudder system, the propeller rotational velocity was adjusted to assure that the advance ratio remained the same or similar under the different ship speeds. For the propeller/rudder system with the new PBCFs, the propeller rotational velocity was controlled to yield a similar thrust to the original system at each ship speed. The simulation results show that the optimized PBCFs yielded an improvement in the propeller efficiency under all the different ship speeds. Compared to the original system, the propeller/rudder system with the new PBCFs lowers the torque at each ship speed, and thus improves the efficiency. At each ship speed in the range of 2–2.5 m/s, a propeller efficiency improvement above 1% is achieved by implementing the new PBCFs. The efficiency gain increases slightly as the ship speed increases, e.g., an efficiency gain of 1.00% and 1.04% at the ship speeds of 2.0 and 2.5 m/s, respectively.

Simulations were also performed for different advance ratios in a range of 0.3–1.0, with different ship speeds but a constant rotational velocity. The new optimized PBCFs were found to improve the propeller efficiency for the entire range of the advance ratio. As the advance ratio increased, the PBCFs improved the propeller efficiency more remarkably, e.g., an efficiency gain of 1.05% and 1.19% at the advance ratio of 0.5 and 1.0, respectively.

Such gains in the propeller efficiency by implementing the optimum PBCFs can reduce a remarkable amount of fuel consumption [8,21]. Up to 4–5% fuel saving is reported by using PBCFs on real ships [8].

Finally, to ensure the optimized PBCFs are practicably feasible in real-life applications, a comprehensive yield strength analysis was performed. The results indicate that our optimized design has no structural fatigue issue at all under normal load conditions and can be manufactured and installed on the real propeller boss cap. The results also indicate that in case the PBCFs cannot withstand the loads, one should improve the design of the span height and maximum thickness.

#### 4. Conclusions

A comprehensive theoretical, experimental, and numerical study was performed to optimize the propeller boss cap with fins for cost-effective improvement of energy efficiency of large vessels in shipping. An optimum design of the PBCFs was attained and implemented in a model-scale modern propeller/rudder system, which had no PBCFs in its original design. Under the design operating condition, an efficiency gain of 0.728 percentage

points or 1.043% over the original propeller/rudder system was achieved by the new PBCFs. Similar gains were obtained under off-design operating conditions. The efficiency increase was achieved mainly by the suppressed hub vortex and partly by the extra thrust. Two issues about the efficiency gains are stressed here. One is that the rudder is included in our investigation as it should be. This limits the gains to some extent as the rudder also has an effect on the hub vortex. The other is that our study is for a modern propeller/rudder system on which PBCFs are generally not as effective as on old propellers. Such gains in the propeller efficiency by implementing the optimized PBCFs can achieve up to a few percentages of fuel saving in real ships. The yield strength analysis shows that the optimum design of the PBCFs is not subject to structural failure under normal load conditions and is practicably feasible for industrial vessels. Table 7 not only summarizes the optimum design of the PBCFs for the propeller/rudder system under investigation but also generalizes the optimum design criteria, which are applicable to other propeller/rudder systems for cost-effective energy saving.

**Author Contributions:** Conceptualization, C.K.R. and M.P.S.; methodology, C.Y., C.K.R., M.P.S. and K.W.S.; software, C.K.R., M.P.S. and K.W.S.; validation, C.K.R. and M.P.S.; formal analysis, C.K.R., M.P.S. and K.W.S.; investigation, C.K.R. and M.P.S.; resources, A.E.; data curation, C.K.R., M.P.S. and A.E.; writing—original draft preparation, C.Y.; writing—review and editing, C.Y., C.K.R., M.P.S., A.E. and K.W.S.; visualization, C.K.R. and M.P.S.; project administration, A.E. All authors have read and agreed to the published version of the manuscript.

**Funding:** This research received no external funding.

**Data Availability Statement:** Not applicable.

**Conflicts of Interest:** The authors declare no conflict of interest. The funders had no role in the design of the study; in the collection, analyses, or interpretation of data; in the writing of the manuscript; or in the decision to publish the results.

## References

1. Issa, M.; Ilinca, A.; Martini, F. Ship energy efficiency and maritime sector initiatives to reduce carbon emissions. *Energies* **2022**, *15*, 7910. [[CrossRef](#)]
2. Szelangiewicz, T.; Abramowski, T.; Zelazny, K.; Sugalski, K. Reduction of resistance, fuel consumption and GHG emission of a small fishing vessel by adding a bulbous bow. *Energies* **2021**, *14*, 1837. [[CrossRef](#)]
3. Artyszuk, J.; Zalewski, P. Energy saving by optimizing thrusters allocation during complex ship manoeuvres. *Energies* **2021**, *14*, 4959. [[CrossRef](#)]
4. Krcum, M.; Zubcic, M.; Kastelan, N.; Gudelj, A. Reducing the dimensions of the ship's main switchboard—A contribution to energy efficiency. *Energies* **2021**, *14*, 7567. [[CrossRef](#)]
5. Wu, P.C.; Chang, C.W.; Huang, Y.C. Design of energy-saving duct for JBC to reduce ship resistance by CFD method. *Energies* **2022**, *15*, 6484. [[CrossRef](#)]
6. Kim, K.I.; Lee, K.M. Dynamic programming-based vessel speed adjustment for energy saving and emission reduction. *Energies* **2018**, *11*, 1273. [[CrossRef](#)]
7. Ouchi, K.; Ogura, M.; Kono, Y.; Orito, H.; Shiotsu, T.; Tamashima, M.; Koizuka, H. A research and development of PBCF (propeller boss cap fins). *J. Soc. Nav. Archit. Jpn.* **1988**, *163*, 66–78. [[CrossRef](#)]
8. Hsin, C.Y.; Lin, B.H.; Lin, C.C. The optimum design of a propeller energy-saving device by computational fluid dynamics. *Comput. Fluid Dyn.* **2008**, *1*, 655–660.
9. Ghassemi, H.; Mardan, A.; Ardeshir, A. Numerical analysis of hub effect on hydrodynamic performance of propellers with inclusion of PBCF to equalize the induced velocity. *Pol. Marit. Res.* **2012**, *19*, 17–24. [[CrossRef](#)]
10. Lim, S.S.; Kim, T.W.; Lee, D.M.; Kang, C.G.; Kim, S.Y. Parametric study of propeller boss cap fins for container ships. *Int. J. Nav. Archit. Ocean Eng.* **2014**, *6*, 187–205. [[CrossRef](#)]
11. Mizzi, K.; Demirel, Y.K.; Banks, C.; Turan, C.; Kaklis, P.; Atlar, M. Design optimization of propeller boss cap fins for enhanced propeller performance. *Appl. Ocean Res.* **2017**, *62*, 210–222. [[CrossRef](#)]
12. Gaggero, S. Design of PBCF energy saving devices using optimization strategies: A step towards a complete viscous design approach. *Ocean Eng.* **2018**, *159*, 517–538. [[CrossRef](#)]
13. Seo, J.; Lee, S.; Han, B.; Rhee, S.H. Influence of design parameter variations for propeller-boss-cap-fins on hub vortex reduction. *J. Ship Res.* **2016**, *60*, 203–218. [[CrossRef](#)]
14. Shin, K.W.; Lundgren, E.; Nielsen, J.R. CFD-based optimization of rudder bulb systems. In Proceedings of the World Maritime Technology Conference, Saint-Petersburg, Russia, 29 May–1 June 2012.

15. Shin, K.W.; Andersen, P. CFD analysis of scale effects on conventional and tip-modified propellers. In Proceedings of the 5th International Symposium on Marine Propulsors, Espoo, Finland, June 2017.
16. Celik, I.B.; Ghia, U.; Roache, P.J.; Freitas, C.J.; Coleman, H.; Raad, P.E. Procedure for estimation and reporting of uncertainty due to discretization in CFD applications. *J. Fluids Eng.* **2008**, *130*, 078001.
17. Ogura, M.; Koizuka, H.; Takeshita, T.; Kohno, Y.; Ouchi, K.; Shiotsu, T. A Screw Propeller Boss Cap with Fins. Patent. App. nr 87111052.4; Pub. nr: 0 255 136 A1, (accessed on 3 February 1988).
18. Airfoil Tools. 2021. Available online: <http://airfoiltools.com/index> (accessed on 26 November 2021).
19. Majumder, P.; Maity, S. Numerical analysis of aerofoil shape propeller boss cap fin (PBCF) to improve propeller efficiency. *Int. J. Innov. Technol. Explor. Eng.* **2020**, *9*, 231–238. [[CrossRef](#)]
20. Gaggero, S.; Martinelli, M. Comparison of different propeller boss cap fins design for improved propeller performance. *Appl. Ocean Res.* **2021**, *116*, 102867. [[CrossRef](#)]
21. Tadros, M.; Ventura, M.; Soares, C.G. Optimization procedures for a twin controllable pitch propeller of a ROPAX ship at minimum fuel consumption. *J. Mar. Eng. Technol.* **2022**, 1–9. [[CrossRef](#)]

**Disclaimer/Publisher's Note:** The statements, opinions and data contained in all publications are solely those of the individual author(s) and contributor(s) and not of MDPI and/or the editor(s). MDPI and/or the editor(s) disclaim responsibility for any injury to people or property resulting from any ideas, methods, instructions or products referred to in the content.